Microscopic structure of liquid 1-1-1-2-tetrafluoroethane (R134a) from Monte Carlo simulation†

Hainam Do, Richard J. Wheatley and Jonathan D. Hirst*

Received 19th May 2010, Accepted 6th August 2010
DOI: 10.1039/c0cp00620c

1-1-1-2-tetrafluoroethane (R134a) is one of the most commonly used refrigerants. Its thermophysical properties are important for evaluating the performance of refrigeration cycles. These can be obtained *via* computer simulation, with an insight into the microscopic structure of the liquid, which is not accessible to experiment. In this paper, vapour–liquid equilibrium properties of R134a and its liquid microscopic structure are investigated using coupled–decoupled configurational-bias Monte Carlo simulation in the Gibbs ensemble, with a recent potential [*J. Phys. Chem. B* 2009, **113**, 178]. We find that the simulations agree well with the experimental data, except at the vicinity of the critical region. Liquid R134a packs like liquid argon, with a coordination number in the first solvation shell of 12 at 260 K. The nearest neighbours prefer to be localized in three different spaces around the central molecule, in such a manner that the dipole moments are in a parallel alignment. Analysis of the pair interaction energy shows clear association of R134a molecules, but no evidence for C–H···F type hydrogen bonding is found. The above findings should be of relevance to a broad range of fluoroalkanes.

1. Introduction

Hydrofluorocarbons (HFCs) are now widely accepted alternative refrigerants to ozone-depleting chlorofluorocarbons (CFCs). Partially fluorinated alkanes have the same desirable physical properties as CFCs (*i.e.* low boiling point and high latent heat of vaporization), but without the harmful environmental side effects. In addition, hydrofluoroalkanes are also good lubricants, water- and stain-repellant products, chemical agents, and industrial solvents. The HFCs of particular industrial interest are fluorinated methanes and ethanes. 1-1-1-2-Tetrafluoroethane (R134a) is one of the most commonly used, primarily in domestic refrigeration and automobile heating, ventilation and air conditioning systems. Therefore, its thermodynamic properties and microscopic structure attract much attention.[1–3] In evaluating the performance of refrigeration cycles, knowledge of the vapour–liquid equilibrium is important. Traditionally, such data are usually obtained from experiment or from empirical equations of state. These conventional methods can give accurate vapour–liquid equilibrium properties of pure substances or mixtures of components, but they cannot provide insight into the microscopic nature of the systems.

Computer simulation based on molecular modelling can predict vapour–liquid equilibria of fluids under a wide range of conditions, and also provides insight into their microscopic structure. Simulation can also model conditions under which experimental data are difficult or impossible to obtain. Several techniques have been proposed, such as the NPT + test particle method,[4] Gibbs ensemble Monte Carlo (GEMC),[5] Gibbs–Duhem integration,[6] and histogram reweighting grand canonical ensemble Monte Carlo.[7] Intermolecular potentials play a central role in obtaining accurate predictions of properties and microscopic structures. Molecular potential parameters are often optimized using experimental data for pure systems. The potential parameters can also be determined purely from *ab initio* calculations, or from a combination of *ab initio* calculations and experimental data.

There are several potentials for R134a. Lisal *et al.*[8,9] proposed a set of effective pair potentials for R134a and pentafluoroethane using the Halgren's Buff 14-7 and coulombic functions. In these potentials, only the internal rotation about the C–C bond is taken into account; bond lengths and bond angles are kept rigid. The potential functions are adjusted to reproduce the thermodynamic properties of the saturated liquid. Based on *ab initio* calculations (only for geometry optimization and atomic partial charges), Fermeglia *et al.*[10] developed an all-atom potential model for R134a, which uses the 9-6 Lennard-Jones potential to represent the dispersion and induction energy. A dipolar two-centre Lennard-Jones model was also used to describe the vapour–liquid equilibrium of pure R134a and pentafluoroethane and their mixture.[11–13] Peguin *et al.*[3] developed an all-atom force field using a Lennard-Jones 12-6 function to describe the repulsion and dispersion energy and point charges to describe the columbic energy. This new force field accurately predicts the bulk and interfacial properties of R134a. It reproduces the experimental vapour–liquid equilibrium properties especially well. Since the 12-6 Lennard-Jones potential is the most commonly used potential in computer simulations, this force field is straightforward to combine with established potentials, such as SPC/E for water[14] and EPM for carbon dioxide (CO_2),[15–17] to study these interesting mixtures.

School of Chemistry, University of Nottingham, University Park, Nottingham, NG7 2RD, UK.
E-mail: jonathan.hirst@nottingham.ac.uk

† Electronic supplementary information (ESI) available: (A) the potential parameters for R134a, (B) a description of the growing procedure for R134a, (C) the vapour-liquid equilibrium properties of R134a, and (D) an analysis of the orientation of pair interactions in the first solvation shell. See DOI: 10.1039/c0cp00620c

Besides the thermodynamic properties, the liquid structure of real fluids in general and of R134a in particular is also important from a theoretical point of view. There has been much effort devoted to characterizing the microscopic structure of many substances, including CO_2,[17–19] methylene chloride,[20] and difluoromethane,[21] and mixtures, *e.g.*, CO_2 + methane[22,23] and CO_2 + difluoromethane.[23] However, there has not yet been a similar analysis of R134a, partly due to the lack of accurate potentials. The recent R134a potential of Peguin *et al.*[3] gives us the opportunity to investigate the microscopic structure of this substance. Due to the large electronegativity of the fluorine atom, it is interesting to investigate the possible formation of C–H···F type hydrogen bonding in liquid R134a. In fact, this has been studied for difluoromethane, but no evidence for such hydrogen bonding was found.[21] Our study of a larger molecule (R134a) will augment the previous findings in this regard. Beside the possibility of weak C–H···F hydrogen bonding, other factors can also play an important role in determining the liquid structure of R134a. R134a has a relatively high dipole moment[24] of 2.06 D. Thus, strong dipole–dipole interactions are also expected in liquid R134a. Steric interactions are also an important factor in determining the liquid structure of dipolar liquids.[25] Finally, the distribution (both radial and orientational) of neighbouring molecules around a central molecule gives insight into how R134a molecules pack together in liquid phase. Characterization of R134a should provide insights of relevance to a broad range of fluoroalkanes.

2. Methods

The GEMC technique[5] is employed to investigate the vapour–liquid equilibrium and microscopic structure of R134a. Two phases at equilibrium are simulated at a given temperature with a fixed number of R134a molecules in total. There are two cubic simulation boxes, one for each phase. The thermodynamic requirements for phase equilibrium are that each region should be in internal equilibrium, and that the temperature (T), pressure (P) and chemical potential (μ) of all components should be the same in both phases. The phase equilibrium is achieved by performing three types of trial Monte Carlo (MC) moves: particle displacements (including translating and rotating particles) within each box to satisfy internal equilibrium, volume change to equalize the pressure, and particle transfer to equalize the chemical potentials. The total volume of the system cannot change and an increase in the volume of one box must be matched by a decrease in the volume of the other.

To start a simulation, an equal number of molecules are grown at random positions in both boxes, which introduces overlaps in the initial configurations. The densities of each box are chosen initially to give roughly equal partitioning of the particles between each box once equilibrium is reached. Before the volume change and particle transfer moves take place, 10 000 MC displacement steps are used to remove the overlaps. Calculations within the Gibbs ensemble are then performed to determine the vapour–liquid equilibrium properties of R134a. In all simulations 400 molecules are used. Simulations consist of 100 000 MC cycles. The first 40 000 cycles in each simulation are used to equilibrate the system. Each MC cycle comprises an average of one translation move and one rotation move per molecule, one volume move, and 150 particle transfer moves. In addition, the coupled–decoupled configurational-bias MC (CBMC) method[26] is employed to sample the conformation of R134a *via* regrowth moves, and to enhance the probability of successful particle transfer moves. The number of regrowth and configurational-bias particle transfer moves in each MC cycle are 50 and 100, respectively. Details on how to perform a CBMC regrowth and swap moves are addressed elsewhere.[26,27] Here, we only describe in detail (in the ESI†) how a configuration of R134a is generated in our work.

The production period of each simulation is divided into ten blocks, and the standard deviations of the simulations are calculated from these blocks. The acceptance ratios are 25% to 30% for the particle translations and 78% to 82% for particle rotation within the liquid phase. In the vapour phase, the acceptance ratios for both the particle translations and rotations vary between 80% and 90%. The acceptance ratios for the volume change are between 40% and 85%, and those for regrowth moves are between 14% and 18%. The low acceptance rate for molecule transfer, especially to the liquid phase, is one of the main challenges in the simulations, and this is enhanced by also performing the configurational-bias particle transfers move. The acceptance ratios for the particle transfers are always less than or equal to 0.5% and for configurational-bias particle transfers they vary between 0.1% and 2%.

The simulations use the potential of Peguin *et al.*[3] as summarised in the Introduction and the potential is described in greater detail in the ESI.† A spherical cutoff, r_{cut}, of 10 Å between molecules is used to truncate the Lennard-Jones part of the potential energy. Since the r^{-6} Lennard-Jones term still makes a significant contribution to the interaction energy beyond the cutoff distance, a long-range correction (tail correction)[28] is used, where the long-range energy of a molecule is given by

$$E_{\text{tail}} = \frac{2}{3}\pi\rho(4\varepsilon\sigma^6)r_{\text{cut}}^{-3}, \quad (1)$$

where ρ is the density of molecules in the box, ε is the well depth of the Lennard-Jones potential and σ is the Lennard-Jones core diameter. The r^{-12} term decays rapidly with distance; so a correction to this term is unnecessary. Ewald summation with tinfoil boundary condition is used to calculate the long-range electrostatic interactions.[29]

3. Results and discussion

3.1 Vapour–liquid equilibrium of R134a

We first consider the GEMC simulations of the vapour–liquid equilibrium properties. These are plotted in Fig. 1 (see also Table S3 in the ESI†) with a comparison to previous studies[3] and experiment.[30] In general, the vapour and liquid densities agree with experiment over most of the temperature range, as shown in Fig. 1a. The differences between simulation and experiment are quite small at low temperatures, and increase gradually as the system approaches the critical temperature. In most cases, the differences are within the uncertainties of the

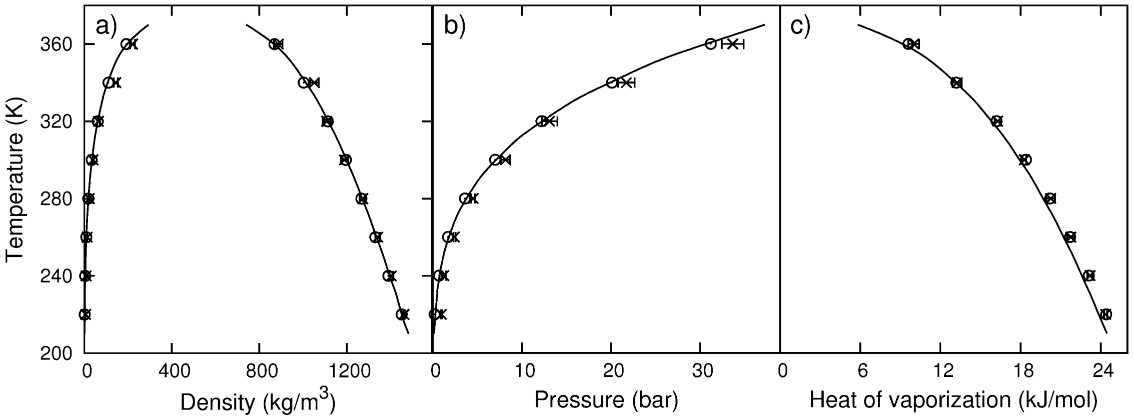

Fig. 1 Vapour–liquid equilibrium coexistence curves (a), temperature–pressure equilibrium curve (b), and the latent heat of vaporization (c) of R134a: our simulations (crosses), calculations of Peguin *et al.*[3] (circles) and experiment[30] (solid line).

simulation results. Due to the finite size effect, GEMC cannot simulate the phase equilibrium properties of any system at the vicinity of the critical point (T_c = 373.9 K). This is a well-known problem and has been addressed elsewhere.[5,31] The simulations slightly overestimate the saturated vapour pressure of R134a (Fig. 1b). However, the deviations are quite small and still within the range of the statistical uncertainties of the simulations (shown in parentheses in Table S3, ESI†). The latent heat of vaporization (Fig. 1c) is satisfactorily predicted at high temperatures, but slightly overestimated at low temperatures.

3.2 Microscopic structure of R134a

Our main goal here is to investigate the liquid structure of R134a. We take the simulated data of saturated liquid R134a at 260 K as an example to probe its intermolecular structure. Two established methods, which are often used to analyze the microscopic structure of substances, are employed. The radial distribution functions (RDFs) probe the occurrence of an atom at a distance from another atom. Peaks in an RDF are associated with solvation shells or specific neighbours. The orientational distribution function (ODF) gives information about the distribution of average angles between a pair of molecules at a given separation. In addition, we also analyze pair interaction energies.

To begin, we establish the distribution of the conformation of R134a molecules under these conditions, as the CF_3 and the CH_2F groups can freely rotate about the CC bond. The ensemble of configurations collected in the course of the simulations is analyzed. Fig. 2a shows the distribution of the average FCCF dihedral angles at 260 K. There is a sharp peak at 180° ($\cos\phi = -1$) and a lower one at about 60°, *i.e.*, the FCCF dihedral angles of R134a have a preference for both 60° and 180°. Snapshots of the conformation of R134a are shown in Fig. 2b. This conformation is similar to ethane and is the most stable, as all six CF and CH bonds are furthest from each other, minimizing steric interactions.

In order to investigate the relative importance of the different types of interactions, we calculated separate contributions of

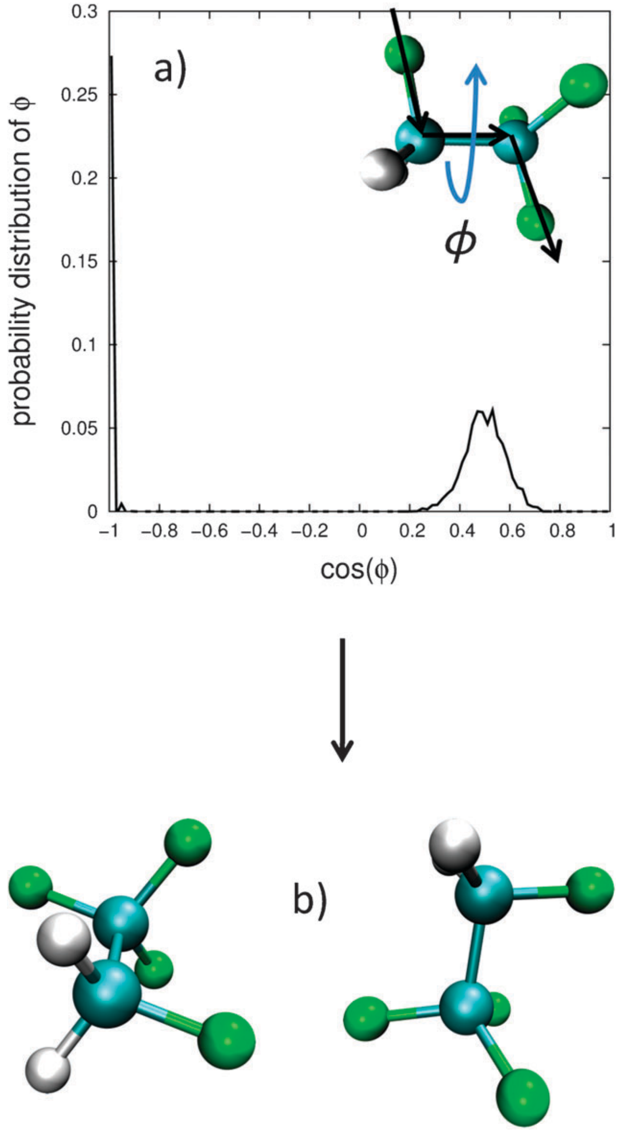

Fig. 2 Probability distribution of the FCCF dihedral angles of R134a (a) and snapshots of the conformation of R134a (b) at 260 K.

Table 1 Intermolecular energy of liquid R134a

T/K	U_L/kJ mol^{-1}	U_{LJ}/kJ mol^{-1}	U_C/kJ mol^{-1}
220	−22.99 (0.11)	−16.13 (0.10)	−6.86 (0.09)
240	−21.66 (0.13)	−14.90 (0.10)	−6.76 (0.09)
260	−20.33 (0.17)	−14.61 (0.11)	−5.72 (0.08)
280	−18.96 (0.27)	−14.06 (0.09)	−4.90 (0.08)
300	−17.37 (0.13)	−12.54 (0.13)	−4.83 (0.10)
320	−15.97 (0.19)	−11.96 (0.11)	−4.01 (0.17)
340	−14.94 (0.18)	−10.46 (0.20)	−4.48 (0.19)

T: temperature, U_L: configurational intermolecular energy in the liquid phase, U_{LJ}: configurational intermolecular energy due to Lennard-Jones interaction in the liquid phase, U_C: configurational intermolecular energy due to electrostatic interaction in the liquid phase. The numbers in parentheses indicate the statistical uncertainties.

the Lennard-Jones and electrostatic terms (U_{LJ}, U_C) to the total intermolecular interaction energy at different temperatures (Table 1). The electrostatic energy accounts for about 30% of the total, which suggests that dipole interaction is not dominant. Instead, liquid R134a seems to be dominated by dispersion energy, as the Lennard-Jones interaction accounts for about 70% of the total intermolecular interaction energy.

The pair interaction energy distribution is computed from the ensemble of individual molecule–molecule interactions. We have determined the distribution of the U_{ij} pair interaction energies for the saturated liquid at three different temperatures, 220 K, 260 K and 340 K (Fig. 3). All curves have a shoulder at about −2 kJ mol^{-1}, on the attractive side of the main peak. This shoulder is a sign of the association of the molecules, which could arise from weak C–H···F hydrogen bonding or simply dipolar association.[21] However, the RDFs of the H–F interactions show no evidence of specific interaction between hydrogen and fluorine, which suggests that C–H···F hydrogen bonding cannot be the dominant form of the molecular association. Similar shoulders also appear on the probability distribution of pair energies of difluoromethane, but no C–H···F hydrogen bonding is found either.[21] Analogous observations have been made for formic acid,[32] as a result of C–H···O hydrogen bonding, and for liquid acetone[33] and acetonitrile,[34] due to the dipolar association of the molecules. Fig. 4 shows the lowest pair energy encountered in the simulation. The angle between the dipole moment of the two molecules is 104°, indicating that the dipole–dipole interaction does not play an important role in the determination of this dimer arrangement.[21]

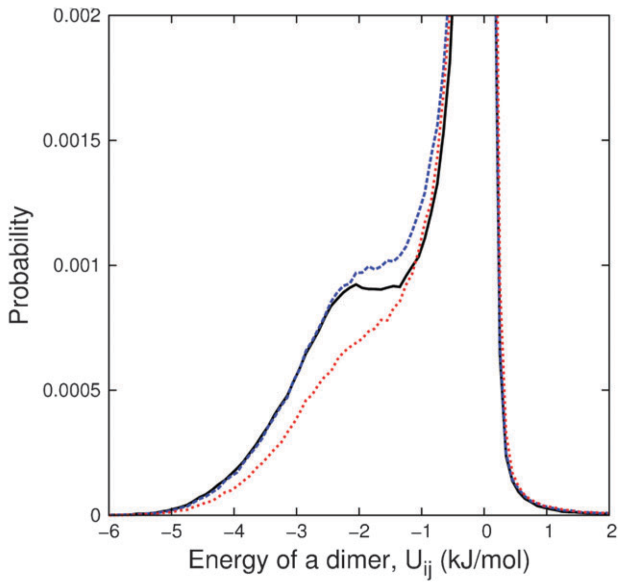

Fig. 3 Probability distribution of the pair interaction energy of R134a molecules at 220 K (solid line), 260 K (dashed line) and 340 K (dotted line).

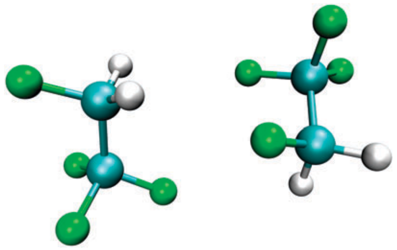

Fig. 4 Configuration of the R134a dimer with the lowest interaction energy (−6.518 kJ mol^{-1}) taken from simulation at 260 K.

Fig. 5 shows the RDF of R134a molecules, considering one site per molecule at 260 K. For convenience, we identify the centre of the molecule, which we refer to as CoCC, as the midpoint of the CC bond rather than the molecular centre of mass. The RDF exhibits all the features of a closely packed system, given the size of the molecule. There are two peaks, at CoCC–CoCC distances of about 5 Å and about 9.5 Å. The ratio of the positions of the second and first peak is about 1.9, and the ratio of the first minimum and the first peak position is about 1.4, which is similar to that of liquid argon. These ratios are also found for other small molecules, such as methane, CO_2, and difluoromethane.[21,23] The coordination number is about 12, which is similar to that of liquid methane, CO_2, and difluoromethane.[21,23] The integration of g_{C2C2}, g_{C3C3}, and g_{HH} up to their first minimum also yields a coordination number of about 12. To have a clearer picture of the arrangement of pairs of atoms in the system, we calculate the RDFs, considering all interaction sites (Fig. 6). In the first solvation shell, the CC interactions are the most structured, as indicated by the

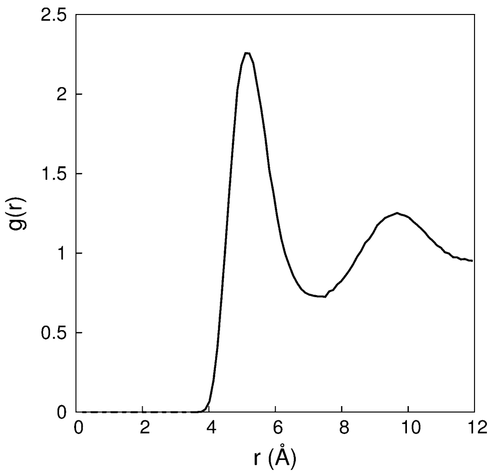

Fig. 5 Radial distribution function of saturated liquid R134a, considering one site (centre of the CC bond) per molecule at 260 K.

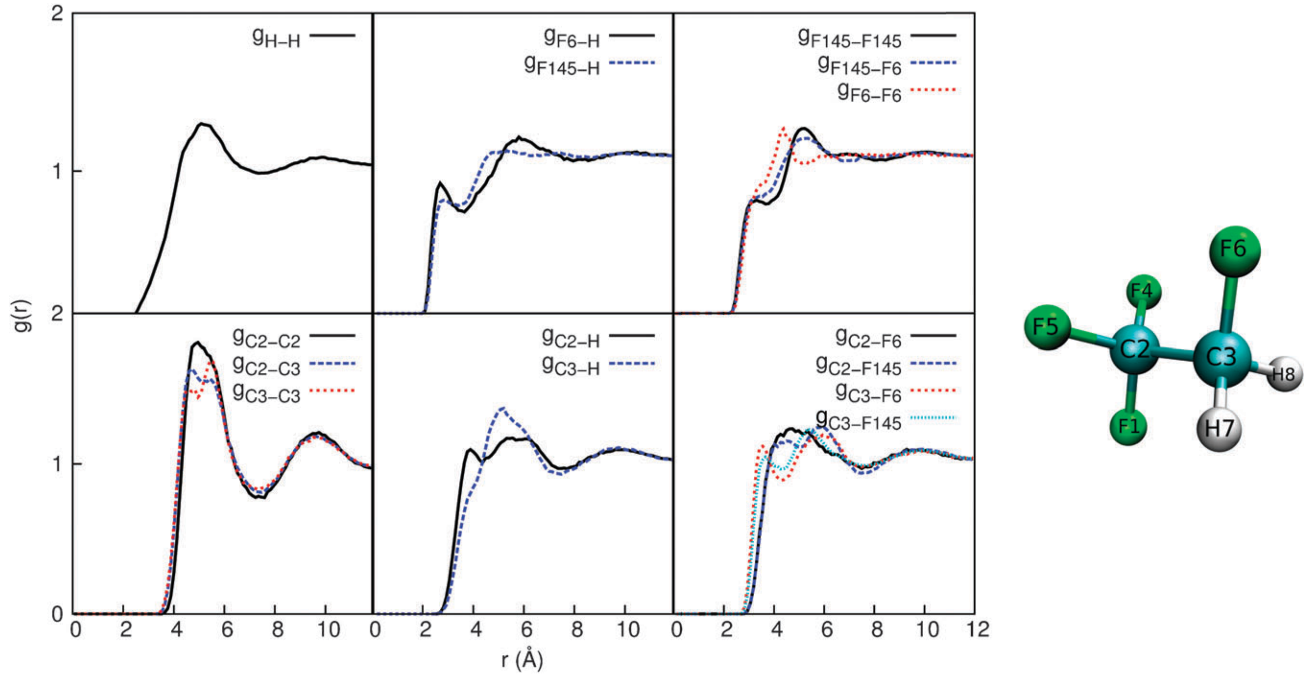

Fig. 6 Radial distribution functions of R134a, considering all interaction sites at 260 K.

narrow and sharp peaks (g_{C2C2}, g_{C2C3}, g_{C3C3}). This shows that carbon atoms aggregate together at about 5 Å. In contrast, the other interactions are not very structured; their peaks are low and broad.

Augmenting the RDFs, we use the ODFs to characterise the environments around each molecule in the liquid. Fig. 7a shows the distribution of the angle between C2C3 vectors and the intermolecular vectors CoCC–CoCC of pairs of R134a molecules at 260 K. This distribution tells us how R134a molecules are positioned around a reference molecule in the liquid. In this figure, the vertical axis represents the distance between the centres (CoCCs) of pairs of R134a molecules. There are three maxima, which correspond to the first solvation shell. Two are located at a CoCC–CoCC distance of about 5.2 Å and angles of 0° and 180°, with a coordination number of two for each peak. A larger peak appears at about 5.0 Å and an angle of about 90°, with a coordination number of six. Thus, R134a molecules preferentially populate a circle of radius 5.0 Å around the midpoint of the CC bond of the central molecule. They also prefer to sit above and below the central molecule (Fig. 7b).

In order to investigate further the orientations of the neighbouring molecules, we divided the space around a reference molecule into four spaces: π_F, π_H, π_T and π_B (Fig. 8). A plane that cuts through C2C3 and is perpendicular to the C2C3F6 plane is used to separate the spaces π_F and π_H. One would expect that the orientations of the molecules in the four spaces would be different. Therefore, we analyze the preferred orientations of the neighbouring molecules in all spaces separately. In the space π_F, the C2C3 vectors of the nearest neighbours in the first solvation shell have a preference for a perpendicular alignment (Fig. S2a, ESI†), while dipole vectors in this space have a preference for a parallel alignment, with some variation up to 30° with each other (Fig. S2b, ESI†). Like the dipoles, the C3F6 bonds also prefer a parallel alignment, but with greater variation (Fig. S2c, ESI†). Combining the information from these three figures, we can deduce the preferred orientations of the neighbouring molecules in the π_F space of the first solvation shell, as shown in Fig. S2d ESI.† In the space π_H (Fig. S3, ESI†), the distribution of the angle between C2C3 vectors is the same as that in the π_F space. However, at short distances, the C2C3 vectors have a preference for antiparallel alignment, but this alignment disappears quickly as the distance between molecules increases. We do not observe this alignment of the angle between C2C3 vectors in the π_F space. Both the dipole vectors and the C3F6 bonds in this space prefer a parallel alignment. Unlike in the spaces π_F and π_H, the C2C3 vectors of the nearest neighbouring molecules prefer a parallel alignment in the π_T space (Fig. S4a, ESI†). The distribution of the average angle between dipoles (Fig. S4b, ESI†) also reveals that the dipoles prefer to be parallel to each other and so do the C3F6 bonds (Fig. S4c, ESI†). A similar orientation is preferred by the molecule that sits at the bottom of the central molecule in the first solvation shell (Fig. S5, ESI†). A snapshot of the first solvation shell of saturated liquid R134a at 260 K is shown in Fig. 9.

4. Conclusion

We have used coupled–decoupled CBMC simulations[26] in the Gibbs ensemble to study the microscopic structure of saturated liquid R134a. We also calculated the vapour–liquid equilibrium properties for R134a. The potential employed has been recently published,[3] where it was used in grand canonical MC (GCMC) simulations to determine vapour–liquid equilibrium properties. Both GCMC and GEMC methods yield good agreement with experiment, which implies that the methods

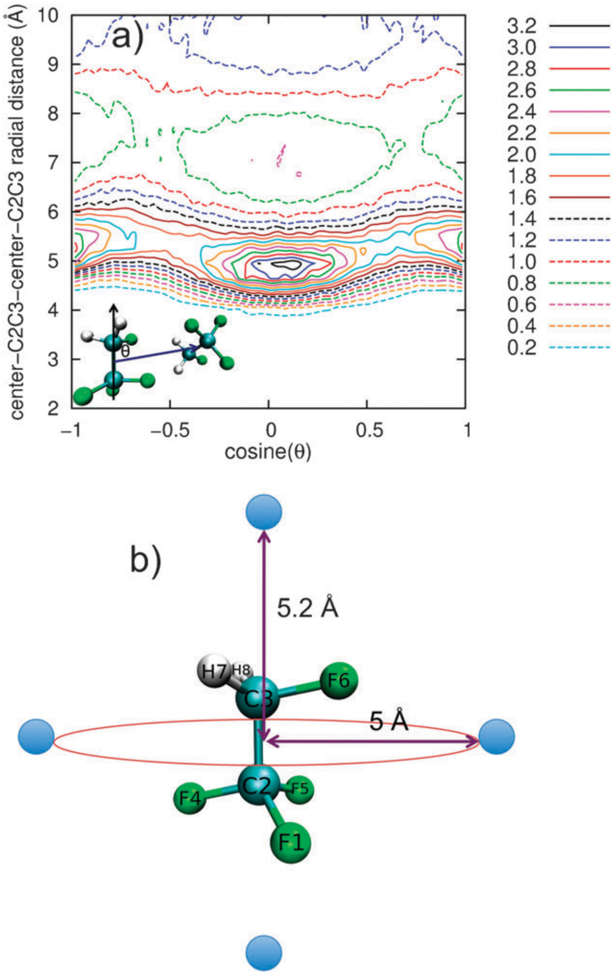

Fig. 7 (a) Distribution of the average angle between C2C3 vectors and CoCC–CoCC vectors in liquid R134a at 260 K. (b) Schematic of the distribution of the midpoint of the CC bonds around a central molecule.

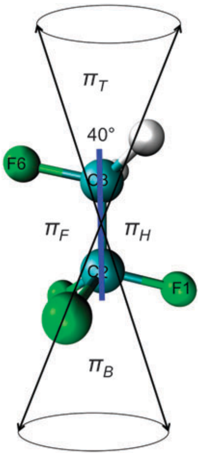

Fig. 8 Schematic of the division of the space around the reference molecule. π_F is the space that contains the fluorine atom of the CH_2F group, π_H is the space that contains the hydrogen atoms of the CH_2F group, π_T is the space above the reference molecule, and π_B is the space below the reference molecule.

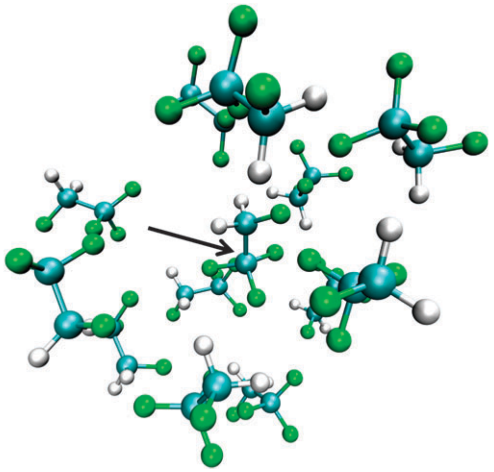

Fig. 9 Snapshot of the first solvation shell of R134a at 260 K. The arrow points to the central molecule.

are effective and the intermolecular potential is relatively accurate. Knowledge of vapour–liquid equilibrium is important in evaluating the performance of refrigeration cycles, because the two main processes in refrigeration cycles are the condensation and the evaporation of the refrigerants. The simulations of this system will augment empirical and experimental data in this regard.

Data for saturated liquid R134a at 260 K are taken from the GEMC simulations to analyze its microscopic structure. The RDFs reveal that the ratio of the positions of the second and first peaks, and the ratio of the first minimum and the first peak position are similar to that of liquid argon. The coordination number is about 12, which is similar to that of liquid methane, CO_2, and difluoromethane. The CC interactions are the most structured, whereas the other interactions are not very ordered. The ODFs reveal that the dipole moments of liquid R134a of the nearest neighbours in the first solvation shell have a preference for a parallel alignment. This is also characteristic of liquid CH_2F_2. The alignments of the neighbouring molecules in the π_F and π_H spaces around the central molecule are different. Particularly, in the π_H space, the C2C3 bonds have a preference for anti-parallel alignment at short distance (4.7 Å), which is not observed in the π_F space. The alignments of the neighbouring molecules above and below the central molecule are more or less the same. In liquid R134a, the electrostatic energy only accounts for about 30% of the total intermolecular interaction energy, whereas the Lennard-Jones interaction accounts for about 70%. The association of the molecules is found from the pair interaction energy analysis, but there is no evidence of weak C–H–F hydrogen bonding.

As computational power continues to improve, we expect to see more *ab initio* force fields in the future. This will allow us to obtain the thermodynamic properties from pure theory, and also provide a more comprehensive understanding of the molecular interactions at a microscopic scale. The mixing rule is a very convenient approximation for unlike interactions, but there is no guarantee that it works for every unlike interaction. Strictly speaking, we should calculate the potential parameters for every single interaction in the system, ideally from first principles and use non-additive potentials. Work along these lines is in progress.[35,36] Nevertheless, the semi-empirical force field employed in our work gives satisfactory agreement with experiment for vapour–liquid equilibrium properties, and also gives us the opportunity to analyze for the first time the microscopic structure of R134a—an important industrial substance.

Acknowledgements

We thank the University of Nottingham High Performance Computing facility for providing computer resources and the Engineering and Physical Sciences Research Council for funding (Grant No. EP/E06082X). We thank Dr Mark Oakley, Prof. Martyn Poliakoff, and Dr Jie Ke for useful discussions.

References

1 P. Selvam, R. P. S. Peguin, U. Chokshi and S. R. P. da Rocha, *Langmuir*, 2006, **22**, 8675.
2 R. P. S. Peguin, L. Wu and S. R. P. da Rocha, *Langmuir*, 2007, **23**, 8291.
3 R. P. S. Peguin, G. Kamath, J. J. Potoff and S. R. P. da Rocha, *J. Phys. Chem. B*, 2009, **113**, 178.
4 J. Vrabec and J. Fischer, *Mol. Phys.*, 1995, **85**, 781.
5 A. Z. Panagiotopoulos, *Mol. Phys.*, 1987, **61**, 813.
6 D. A. Kofke, *Mol. Phys.*, 1993, **78**, 1331.
7 J. J. Potoff and A. Z. Panagiotopoulos, *J. Chem. Phys.*, 1998, **109**, 10914.
8 M. Lisal and V. Vacek, *Fluid Phase Equilib.*, 1997, **127**, 83.
9 M. Lisal, R. Budinskey, V. Vacek and K. Aim, *Int. J. Thermophys.*, 1999, **20**, 163.
10 M. Fermeglia, M. Ferrone and S. Pricl, *Fluid Phase Equilib.*, 2003, **210**, 105.
11 R. Budinskey, V. Vacek and M. Lisal, *Fluid Phase Equilib.*, 2004, **222**, 213.
12 J. Stoll, J. Vrabec and H. Hasse, *J. Chem. Phys.*, 2003, **119**, 11396.
13 J. Vrabec, Y. Huang and H. Hasse, *Fluid Phase Equilib.*, 2009, **279**, 120.
14 H. J. C. Berendsen, J. R. Grigera and T. P. Straatsma, *J. Phys. Chem.*, 1987, **91**, 6269.
15 J. G. Harris and K. H. Yung, *J. Phys. Chem.*, 1995, **99**, 12021.
16 Z. Zhang and Z. Duan, *J. Chem. Phys.*, 2005, **122**, 214507.
17 Y. Zhang, J. Yang and Y. Yu, *J. Phys. Chem. B*, 2005, **109**, 13375.
18 A. Idrissi, P. Damay and M. Kiselev, *Chem. Phys.*, 2007, **332**, 139.
19 A. Idrissi, I. Vyalov, P. Damay, A. Frolov, R. Oparin and M. Kiselev, *J. Phys. Chem. B*, 2009, **113**, 15820.
20 P. Jedlovszky, *J. Chem. Phys.*, 1997, **107**, 562.
21 P. Jedlovszky and M. Mezei, *J. Chem. Phys.*, 1999, **110**, 2991.
22 I. Skarmoutsos and J. Samios, *J. Mol. Liq.*, 2005, **125**, 181.
23 H. Do, R. J. Wheatley and J. D. Hirst, *J. Phys. Chem. B*, 2010, **114**, 3879.
24 *HFA Propellants for Medical Use*, Solvay Fluor und Derivate GmbH, Solvay, Hannover, 2003, p. 43.
25 T. Radnai, I. Bako, P. Jedlovszky and G. Palinkas, *Mol. Simul.*, 1996, **16**, 345.
26 M. G. Martin and J. I. Siepmann, *J. Phys. Chem. B*, 1999, **103**, 4508.
27 B. Smit, S. Karaborni and J. I. Siepmann, *J. Chem. Phys.*, 1995, **102**, 2126.
28 D. Frenkel and B. Smit, *Understanding Molecular Simulation: From Algorithms to Applications*, Academic Press, San Diego, 2002.
29 M. P. Allen and D. J. Tildesley, *Computer Simulation of Liquids*, Clarendon Press, Oxford, 1987.
30 E. W. Lemmon, M. O. McLinden and M. L. Huber, *Thermodynamic and Transport properties of Refrigerants and Refrigerant Mixtures*, Standard Reference Database 23-Version 7.0, NIST, 2002.
31 B. Smit, P. D. Smedt and D. Frenkel, *Mol. Phys.*, 1989, **68**, 931.
32 P. Jedlovszky and L. Turi, *J. Phys. Chem. B*, 1997, **101**, 5429.
33 P. Jedlovszky and G. Palinkas, *Mol. Phys.*, 1995, **84**, 217.
34 W. L. Jorgensen and J. M. Briggs, *Mol. Phys.*, 1988, **63**, 547.
35 M. T. Oakley and R. J. Wheatley, *J. Chem. Phys.*, 2009, **130**, 034110.
36 M. T. Oakley, H. Do and R. J. Wheatley, *Fluid Phase Equilib.*, 2010, **290**, 48.